Identification of an inhibitory pocket in falcilysin bound by chloroquine provides a new avenue for malaria drug development

Grennady Wirjanata[1*], Jerzy Michal Dziekan[1*], Jianqing Lin[1,2,3*], Abbas El Sahili[1,2,*], Nur Elyza Binte Zulkifli[1], Josephine Boentoro[1,4], Ka Diam Go[1], Han Yu[1], Anthony Partridge[5], David Olsen[6], Nayana Prabhu[1], Radoslaw M Sobota[7,8], Pär Nordlund[1,7,9], Julien Lescar[1,2,10,#] & Zbynek Bozdech[1#]

[1]School of Biological Sciences, Nanyang Technology University, Singapore 637551

[2]NTU Institute of Structural Biology, Nanyang Technology University, Singapore 637551

[3]Infectious Diseases Horizontal Technology Centre & Singapore Immunology Network, Agency for Science, Technology and Research, 138648, Singapore

[4]Faculty of Science and Technology, Universitas Pelita Harapan, Indonesia

[5]MSD, Singapore

[6]Merck & Co., Inc., West Point, PA 19486 USA

[7]Institute of Molecular and Cell Biology, Agency for Science, Technology, and Research (A*STAR), Singapore 138673

[8]Functional Proteomics Laboratory, Institute of Molecular and Cell Biology, Agency for Science, Technology and Research (A*STAR), Singapore, Singapore

[9]Department of Oncology and Pathology, Karolinska Institutet, Stockholm, 17177 Sweden

[10]Antimicrobial Resistance Interdisciplinary Research Group, Singapore-MIT Alliance for Research and Technology, Singapore 637551

* Equally contributing authors

Corresponding authors: julien@ntu.edu.sg; zbozdech@ntu.edu.sg

Abstract

Despite their widespread use, our understanding of how malaria drugs work remains limited. This includes chloroquine (CQ), the most successful antimalarial ever deployed. Here, we used MS-CETSA and dose-response transcriptional profiling to elucidate protein targets and mechanism of action (MOA) of CQ, as well as MK-4815, a malaria drug candidate with a proposed MOA similar to CQ. We identified falcilysin (FLN) as the target of both compounds and found that hemoglobin digestion was the key biological pathway affected, with distinct MOA profiles between CQ-sensitive and CQ-resistant parasites. We showed that CQ and MK-4815 inhibit FLN proteolytic activity, and using X-ray crystallography, that they occupy a hydrophobic pocket situated within the large peptide substrate binding cavity of FLN. As a key protein in the MOA of CQ, FLN now constitute an interesting target for the development of novel anti-malarial drugs with improved resistance profiles.

Introduction

Malaria remains a major public health problem with > 200 million cases and 400,000 deaths in 2018[1]. Declining efficacy for artemisinin-based combination therapy as the frontline treatment for malaria, is particularly worrisome, given the limited number of clinically-approved treatments and widespread emerging resistance[2-5]. The majority of antimalarial drugs used in the past and in present were derived from phenotypic-based screenings followed by empirical scaffold improvement[6,7]. As a result, knowledge of targets and associated mode of action (MOA) remains fragmentary for most antimalarial drugs. A prime example of this is chloroquine (CQ) that represents by far the most successful antimalarial in history, having saved millions of lives and prevented hundreds of millions of malaria cases[8]. Initially synthesized in 1934, it was not until the 1940s when CQ was deployed worldwide for prophylaxis and treatment of malaria immediately after World War II[9]. Unfortunately, reports of CQ resistance in *P. falciparum* began cropping up in the 1950s across different continents and by the late 1980s CQ resistance has spread to nearly all endemic regions in Asia, Africa, and South America, leading to the discontinuation of CQ use for the treatment of falciparum malaria[10]. Although CQ is no longer used for malaria treatment, its efficacy, safety profile, and cost-effectiveness remain the gold standard for any novel antimalarial[8].

Extensive research over the last four decades links CQ antimalarial activity with its ability to disrupt hemoglobin degradation, a key biological process carried out by the malaria parasites during their intraerythrocytic developmental cycle (IDC). *Plasmodium falciparum*, the deadliest species of human malaria parasites, digests up to 65% of the host-cell hemoglobin through a cascade of proteolytic cleavages occurring within the parasite digestive vacuole (DV)[11]. This releases amino acids for parasite protein synthesis but also free heme which is toxic to the parasite through oxygen radicals generated by free heme[12-17]. As a protective mechanism, *P. falciparum* converts the liberated heme into an inert crystalline form (hemozoin) via lipid[18-20] and protein factors such as histidine-rich protein 2[21] and heme detoxification protein[22-25]. CQ is a diprotic weak base, which, in its unprotonated form, is able to traverse the parasitized erythrocyte membrane traveling along the pH gradient to accumulate in the DV[26]. There, it exerts its main activity through (i) interference with hemozoin formation by direct binding to crystals[27,28], (ii) formation of a complex with heme and (iii) inhibition of hemoglobin binding to falcipain 2, which in turn affects heme formation[22]. Indeed, reduced accumulation in the DV is the main cause of CQ resistance, a consequence of mutations to the *pfcrt* gene (*P. falciparum* Chloroquine Resistance Transporter protein), thus facilitating CQ efflux out of the DV[29,30].

Given its success, numerous efforts have been conducted to develop and/or screen for compounds that mimic CQ antimalarial activity, focusing predominantly on the quinoline scaffold as the key chemical moiety. The best examples include amodiaquine and mefloquine (MFQ) that were deployed for clinical use in the 1970s[26]. More recently, the experimental compound MK-4815, a novel chemotype discovered from the MSD chemical collection, was shown to be effective against both CQ-sensitive (CQS) and CQR parasites and highly efficacious in an animal malaria model[31]. MK-4815 appears to share a CQ-like MOA based on the observation that MK-4815 accumulates to low mM concentration in trophozoite/schizont-infected erythrocytes and interferes with heme polymerization[31]. Altogether, hemoglobin degradation disruption remains of high interest for the development of novel antimalarial compounds and one that would be benefit from a deeper understating of the corresponding underlying molecular processes. In particular, identifying possible protein factors essential for hemoglobin digestion could provide suitable drug targets for novel or improved antimalarials. Here, we used the mass-spectrometry based cellular thermal shift assay (MS-CETSA)[32,33] to identify direct protein targets of CQ and MK-4815. We demonstrate that both drugs bind directly to a hydrophobic pocket of a DV residing metalloprotease, falcilysin (FLN)[34,35], and thereby inhibits FLN protease activity. Our data suggest that inhibition of this protease represents a main aspect of CQ MOA, a feature that can be explored for future drug development.

Results

MS-CETSA identifies falcilysin (FLN) as a protein target of CQ and MK-4815

We used mass-spectrometry based cellular thermal shift assay (MS-CETSA) to identify protein targets of CQ and MK-4815, applying a similar strategy as previously described for identifying targets for quinine and mefloquine[32,33,36] . We first used the Iso-Thermal Dose Response (ITDR) implementation of MS-CETSA that monitors protein thermal stability changes for increasing drug concentrations, at clinically relevant concentrations of CQ (0.5-5 µM). As the anti-malarial activity of CQ requires cellular accumulation in the DV, we first conducted ITDR with live *P. falciparum*-infected erythrocytes. Using the CQ sensitive (CQS) 3D7 strain of *P. falciparum*, we identified a total of eleven proteins: seven at ITDR 51°C (n=1119 proteins) and four at ITDR 57°C (n=1086 proteins), that exhibited a significant thermal stability shift upon one hour exposure to CQ (**Fig. 1A, Figure S1, and Table S1)**. From the eleven identified proteins, falcilysin (FLN; *PF3D7_1360800*) exhibited the most significant shift characterized by the largest increase in abundance along the drug concentrations (ΔAUC) following well-structured sigmoidal profile (R^2 value)[32]. In contrast, CQ failed to induce significant thermal shift of any *P. falciparum* protein in the

CQ resistant (CQR) Dd2 strain of *P. falciparum* (**Fig. 1B**). The Dd2 strain is known to possess up to 10-fold higher EC_{50} for CQ compared to 3D7[29,37]. Hence, the lack of response on the CQR Dd2 strain was rather expected, which in turn indicates that identified proteins in the 3D7 likely represent components of the CQ MOA. Next, we carried out ITDR using MK-4815 to examine whether it has a MOA similar to CQ. In the 3D7 strain, MK-4815 induced significant thermal shifts of eight proteins (n=509 total identified proteins at ITDR of 51°C and n=500 at ITDR of 57°C) (**Fig. 1C, Fig S2, and Table S1**). These proteins did not overlap with those identified in the CQ CETSA with the notable exception of FLN, the protein which exhibited the strongest stabilization amongst the MK4815-induced thermal shifts. CQ and MK-4815 induced similar degree of thermal stabilization effects in FLN, with a maximum of 2-3 fold change in the degree of protein stabilized (expressed in non-denatured protein fraction) compared to untreated (**Fig. 1D and 1F, Table S1**). However, treatment of CQ in the CQR strain Dd2, showed drastically reduced FLN stabilization. Specifically, we observed a maximum of 1.5 fold difference in the degree of protein stabilization compared to untreated and at substantially higher CQ dose (i.e., ~40-fold higher CQ MDT (minimal dose threshold; minimum concentration required to induce thermal stabilization)) compared to 3D7 **(**compare **Fig. 1D and E & Table S1)**, rendering its overall thermal shift below the statistical thresholds (**Fig. 1B**). In contrast to the differences seen in the two cell lines for CQ, MK-4815 exerted equally strong effect on FLN in both CQS 3D7 and CQR Dd2 strains as demonstrated by western blot analysis (**Fig. S3**), suggesting that in *P. falciparum*, MK-4815 is not subjected to the same resistance mechanism as CQ, as previously suggested[38].Taken together, FLN stabilization profiles from both CQS and CQR strains suggest that FLN engagement is indeed related to CQ MOA.

Next, we conducted ITDR experiments using *P. falciparum* total protein lysate, in which altered thermal stability is more likely to originate from a direct drug interactions; as opposed to the cellular situation where downstream drug effects are also often seen in MS-CETSA experiments[39]. In the CQ- and MK-4815-treated proteins lysates from 3D7 and Dd2 strains, ITDR analysis identified unique sets of proteins (n=3-17) with significant shifts in thermal stability (**Fig. S4-S6, Table S1**). Notably, FLN, also exhibited thermal stabilization; however, thermal stabilization was only observed at concentration ~500-1,000 fold higher as compared to intact cell samples in both 3D7 (Intact cell MDT of 6.2 nM vs lysate MDT of 5,840; **Fig. 1D & 1G**) and Dd2 (Intact cell MDT of 259 nM vs lysate MDT of 33,970 nM)(**Fig. 1E & 1H**). The substantial difference in FLN thermal stabilization between lysate and intact cell suggests that drug accumulation inside of the parasite is a pre-requisite for protein engagement. In addition, this also suggests that outside its cellular context, FLN interacts with CQ with relatively comparable affinities either in CQS or CQR parasites from

which cell lysates were prepared. In contrast, FLN engages MK-4815 with similar affinity in the CQS 3D7 protein lysates (MDT = 104.3 nM) and intact cells (MDT = 113 nM) (**Fig. 1F and 1I**).

Taken together, these data support that FLN is a direct protein target for both CQ and MK-4815 contributing to their antimalarial MOA. Moreover, FLN is a possible target for mefloquine (MFQ), which was determined by its thermal stabilization in intact-cells, in our previous study[33]. FLN is a crucial *Plasmodium* metalloprotease that is believed to contribute to the hemoglobin degradation process inside the DV[35,40]. To explore this further, we explored the FLN interactions with CQ, MK4815 and MFQ using a recombinant protein.

CQ, MFQ and MK-4815 bind to FLN and inhibit its proteolytic activity

First, we conducted isothermal titration calorimetry (ITC) measurements with recombinant FLN (**Fig. 2A and Fig. S7**). The ITC results showed a 1:1 interaction and Kd values of 1.79 µM (±0.306 µM) for MK-4815, 116 µM (±18.8 µM) for CQ, and 26.7 µM (±8.6 µM) for MFQ, which agree with relative thermal stabilization values (i.e., EC_{50}) obtained from ITDR experiments (**Table S1**). Enthalpic contributions dominate the MK-4815–FLN interaction (with ΔH=-4.43±0.117 kcal/mol and -TΔS=-3.42 kcal/mol), whilst entropic contributions are proportionally higher for the CQ-FLN interaction (with ΔH=-2.37±0.251 kcal/mol and -TΔS=-3.00 kcal/mol). This agrees with the observation of a direct hydrogen bond established by MK-4815 with FLN (see below). As a negative control we tested artemether, an endoperoxide antimalarial with a chemical structure clearly distinct from the structures of CQ, MFQ, and MK-4815, does not interact with FLN (**Fig. S8**).

Given the ability of CQ, MFQ, and MK-4815 to bind FLN *in vitro* and in intact live cells, we next tested whether binding led to inhibition of FLN protease activity using a ten amino-acid peptide substrate derived from the hemoglobin sequence[40]. All three compounds tested inhibit FLN proteolytic activity both at pH 5.2 and 7.2, with IC_{50} values of 1.85 µM, 56.94 µM and 73.36 µM at pH 7.2 for MK-4815, CQ and MFQ, respectively (**Fig. 2B**). These measurements fall within the range of EC_{50} values obtained from lysate ITDR (**Table S1**), showing that FLN activity is inhibited at compound concentrations expected in DV at therapeutic doses of these drugs. A Lineweaver-Burke plot shows that FLN inhibition by CQ and MK-4815 is noncompetitive (**Fig. 2C**) with a decrease in the V_{max} of the reaction whilst the Km value is not affected. This mode of inhibition is consistent with the observation that the binding pocket shared between the three inhibitors is at a distance of 14 Å from the active site (see below).

Crystal structures of CQ, MK-4815 and MFQ bound to FLN

We obtained co-crystal structures of FLN bound to CQ, MFQ and MK-4815 at 1.82, 1.55 and 1.9 Å resolution, respectively (**Table S2**). In the closed conformation captured, the large reaction chamber of the active site occupies a volume of 10,886 Å which is fully enclosed by the N and C terminal halves of the protein. The M16 protease active site contains a catalytic Zinc ion tetrahedrally coordinated by His129 and His 133, from the inverted 129-HXXEH-133 motif, Glu243 and a water molecule (**Fig 3A**). For all three compounds, clear residual electron density at a distance of ~14 Å away from the metalloprotease active site was present in a hydrophobic pocket lined by residues Phe82, Phe527, Ile 544 and Phe545 (**Fig. 3C-E**). The chloride moiety of CQ points towards this pocket and establishes a halogen bond with the phenyl ring of Phe545, a residue strictly conserved in other *Plasmodium* FLN proteins such as FLN from *P. vivax* and *P. malariae* (**Fig. 3C and S9**). Parameters defining this interaction fall within the range of tabulated halogen-pi electron (C-Cl---π) interactions[41] : (i) the distance between the Cl atom and the centroid of the Phe545 phenyl ring is 4.1 Å, (ii) the angle between the CQ and F545 aromatic rings is 69.9˚ and (iii) the distance between the two rings centroids is 7.1 Å. Thus, this halogen-pi electron interaction plays a key role to orient and stabilize CQ inside the FLN catalytic chamber (**Fig. 3C**). Several aliphatic and aromatic residues Phe82, Ile513, Leu514, Ala517, Phe527 and Ile544 further contribute to CQ-FLN binding via Van der Waals and hydrophobic interactions (**Fig. 3C**). MFQ, which binds to the same pocket as CQ establishes hydrophobic interactions between its six fluorine atoms and aromatic residues of the pocket including Phe545, Phe82 and Phe527 (that also makes contact with CQ), while Phe44, Leu417, Ile510, Ile513, Leu514, Ala517 and Ile544 establish additional hydrophobic interactions not seen in the FLN-CQ complex (**Fig. 3D**). A water molecule coordinated by Asp451 makes a bridge with the hydroxyl moiety of MFQ. In contrast, MK-4815 does not make direct interaction with the cluster of Phe residues (Phe527, Phe544 and Phe545), but rather establishes hydrophobic interactions with Leu417, Ile510 and Ile513, Leu514 and Ala517 via its two tri-methyl groups on its "hydrophobic side" (**Fig. 3E**). On its other more "polar side", its hydroxyl group hydrogen bonds with Glu530 and, as seen for MFQ, the amide group of MK-4815 hydrogen bonds with Asp451 via a bridging water molecule.

Modelling the structure of FLN in complex with an amyloid peptide substrate, based on the experimental structure of human presequence protease PreP (PDB access code: 4NGE), indicates possible steric hindrance with peptide substrates longer than 15 amino acids (**Fig. 3B**). Hydrophobic residues of a peptide substrate were seen to be anchored precisely in the cavity where CQ is bound and this cavity was named "hydrophobic exosite" [42]. Therefore, inhibitors binding at this position

could reduce the affinity of longer peptide substrates, impairing FLN enzymatic activity. Although in available crystal structures of M16C metalloprotease (PDB codes: 2FGE, 4NGE, 4RPU)[42], only the closed conformations of M16 metalloproteases is represented, a transition between closed and open conformation in solution must occur to allow substrate entry, while the closed conformation is conducive to peptide cleavage and at the end of the cycle, FLN must reopen to release cleaved peptides. This cycle between open and closed forms was shown experimentally using SAXS for PreP[42] whose structure is closely superimposable with FLN (r.m.s.d. of 2.5 Å for 935 overlapped residues). In addition to direct competition with substrate binding, one possibility accounting for the observed enzymatic inhibition is that upon CQ or MK-4815 binding, the conformation of FLN becomes locked in a closed form.

CQ, MK-4815, and MFQ share MOA via interference with hemoglobin digestion

To shed further light on the cellular response to these drugs, we carried out dose-response transcriptional profiling (DRTP) to analyze transcriptional responses of *P. falciparum*. Briefly, genome-wide transcriptional patterns were monitored in parasites treated for 6 hours with a range of drug concentrations as previously described[43]. Overall, we identified 151, 597, and 200 genes upregulated and 106, 293, and 58 genes downregulated in the CQS 3D7 strain upon treatment with CQ, MK-4815, and MFQ, respectively (**Fig. 4A, Supplementary data 1**). In the CQR Dd2 strain, 6 and 178 genes are upregulated and 11 and 293 genes were downregulated upon treatment with CQ and MK-4815, respectively. The severely reduced transcriptional response of Dd2 to CQ (6 up +11 down = 17 genes differentially expressed) is consistent with the CETSA results (**Fig. 1B**) and also reflects the CQR status of this strain[44] suggesting that the CQ resistance mechanism prevents cytotoxic activity of the drug within the parasite cell. The majority of genes are being up- or down-regulated within the range of effective *in vitro* IC_{50} values and where the parasites are treated for the same duration (i.e., **Fig. 4A and Fig. S10**), indicating that the transcriptional changes were due to compound-specific actions. Analysis of overlapping genes between drug treatments and gene ontology-based functional enrichment revealed similarities in the transcriptional response to the three drugs with genes involved in rRNA processing, proteins folding, ribosomal biogenesis commonly upregulated; and a downregulation of genes linked to GTPase signaling, phosphate ion transport and translational initiation (**Fig. 4B-C, Supplementary data 2 and 3**). Crucially, hemoglobin digestion was overrepresented amongst the genes upregulated in CQ and MK-4815 treated 3D7 CQS parasites (**Fig. 4C**). A closer inspection of genes involved in the hemoglobin digestion pathway revealed that CQ caused upregulation in almost all genes involved in the main

hemoglobin proteolytic cascade, including falcipains, plasmepsins, aminopeptidases, and heme detoxification protein (HDP) (**Fig. 4D**). Some of these genes were also upregulated in MK-4815- and MFQ-treated 3D7 CQS and MK4815 Dd2 CQR parasites, suggesting that the FLN inhibition mediated by these compounds also affect hemoglobin digestion. Conversely, hemoglobin digestion genes were largely unaffected in the CQ-treated Dd2 CQR strain which is consistent with the lack of the drug effect in these parasites. In addition to the genes directly involved in the hemoglobin digestion process, two DV transmembrane transporters involved in CQ and MFQ resistance, *pfcrt* and *pfmdr1*, exhibited similar transcriptional response **(Fig. 4D)**. Upregulation of *pfcrt* and *pfmdr1* in MK-4815 treated parasites is particularly interesting and suggests a tight link between these two transmembrane transporters with hemoglobin digestion but without inducing resistance towards this compound.

To test the overlap in their anti-malarial activity, we used isobologram analysis to uncover the synergy or antagonism between CQ and MK-4815, indicative of a common target. In addition we use o-phenanthroline (PHEN), a known zinc chelator and FLN inhibitor [45] to test its involvement in the shared MOA. Essentially, CQ was observed to show antagonism with MK-4815 and PHEN in 3D7, with a mean FIC index of 1.67 and 1.36, respectively. This is in agreement with competition for a shared binding site within the FLN peptide binding cavity and points to similarity in their MOA (**Fig. 2E**). In contrast, in Dd2 strain, combination of CQ/MK-4815 showed an additive effect (mean FIC = 1.04) and a less pronounced antagonism with a CQ-PHEN combination (mean FIC = 1.21) **(Fig. 4E)**. Combination of MK-4815/PHEN in both 3D7 and Dd2 strains was found to be additive, with a FIC index of 1.01 and 1.08, respectively (**Fig. 4E**). Taken together, the transcriptional responses and the isobologram analyses are in a good agreement with a model in which common inhibition of FLN by CQ, MK-4815 and (to some degree) MFQ play a key role in the drugs MOA via disruption of hemoglobin degradation.

Discussion

Here we provide evidence that during its cytotoxic action on *P. falciparum* parasites, CQ binds to FLN and that this interaction leads to the inhibition of FLN proteolytic activity. This suggests that FLN plays a major role in the CQ MOA. The main site for FLN biological activity is the DV, where FLN participates in hemoglobin degradation via its metalloprotease activity[34,35,40,46]. The DV is also the main site of the CQ cytotoxic activity mediated by its interference with hemozoin formation that leads to increased levels of free heme, causing oxidative stress and subsequent parasite death. For that, CQ must accumulate in the DV to reach mM concentrations which are

achieved even in the presence of low μM external drug concentrations[47]. Here, we show several characteristics of CQ-FLN interaction consistent with this model. First, CQ exhibits relatively low affinity to FLN with K_d=115 μM and IC_{50} values of 56.94 μM and 206.7 μM at pH 7.5 and 5.2, respectively, with the latter value being relevant to the acidic environment within the DV. Hence, CQ must reach millimolar concentrations within the DV to achieve FLN inhibition. This is consistent with the current view of the CQ MOA that such high accumulation of CQ in the DV is essential[47-50]. Second, PfCRT-mediated efflux of CQ is known to lower its accumulation in the DV of CQR strains from *P. falciparum*[51-53]. This is consistent with a lack of FLN-CQ engagement in the CQR Dd2 strain that most likely reflects the reduced CQ accumulation that is thought to be 3-10 fold lower in this particular strain[50,53-55]. Finally, there is a direct association between FLN-CQ engagement and transcriptional upregulation of genes involved in hemoglobin degradation that is believed to be the main functional assignment of FLN [26,46,49,54,56-59]. This was also observed for MFQ and MK-4815, which also bind FLN, but not for CQ in the CQR Dd2 strain in which FLN-CQ interaction is severely reduced. The transcriptional upregulation of hemoglobin degradation factors induced by all three tested FLN ligands further strengthen the role of this protease in the quinoline drug MOA.

How inhibition of FLN proteolytic activity translate into the parasite's death remains to be fully investigated. However, several observations link CQ MOA with the hemoglobin degradation. CQ treatment leads to marked accumulation of undigested hemoglobin levels [56], long-chain hemoglobin-derived peptides[60], and di-/tri-peptides[61], indicating disruption in the hemoglobin digestion cascade. In the DV, FLN is likely to be present in a hemozoin formation complex along with HDP, falcipains, and plasmepsins[22]. Although the role of FLN in this complex is unknown, it is possible that the proteolytic activity of FLN plays an important role in hemozoin formation and heme detoxification. Apart from the DV, FLN has been shown to accumulate in the apicoplast, in addition to a minor pool in the mitochondrion, where in the apicoplast it functions to cleave free signal transit peptide which otherwise could insert into membrane lipid bilayers and disrupt organelle function[45]. The apicoplast has garnered attention as a drug target in recent years following the discovery of its essential function in providing the parasites with a number of important cofactors (reviewed in McFadden and Yeh[62]). However, at this point it is not known whether the binding of these compounds to apicoplast-based FLN will contribute to their respective cytotoxicity, but considered that apicoplasts are not similarly acidic as DV, it is less likely that at least CQ, accumulate to the concentrations required to inhibit apicolplast-based FLN.

In recent years, MS-CETSA has garnered attention as a powerful tool to study drug target engagement. The CETSA methodology and its variants were originally developed to assist in anti-cancer drug target discovery efforts[39,63]; however, the use of this methodology has now been expanded to study drug target engagement in human pathogens, such as *E. coli*[64], toxoplasma[65], and *P. falciparum*[32,33,66,67]. In our previous work, we demonstrated the value of CETSA for antimalarial drug deconvolution by identifying PfPNP as a direct molecular target of QN but also MFQ[33]. Here, we identified FLN as a direct molecular target of CQ, MK-4815, and MFQ. Based on this, target based screening and structure-based drug development would now allow for the development of more effective compound with novel and improved resistance profiles.

Acknowledgement

This work was supported by the Singapore Ministry of Education AcRF Tier 1 grant #RG34/19 (S); Tier 3 grant # MOE2019-T3-1-007 and Singapore National Medical Research Council grant #NMRC/OFIRG/0040/2017

Author contributions

Z.B. and J.L. conceived and developed the idea for this article. G.W., J.M.D., J.Q.L., and A.E.S. wrote the manuscript and performed data analysis. G.W., J.M.D., J.Q.L., A.E.S., N.E.B.Z., J.B., K.D.G., and H.Y. carried out experimental work for the experiments presented. G.W., J.M.D., J.Q.L., A.E.S., A.P., D.O., N.P., R.M.S., and P.N. contributed to the development of experimental protocol and reagents in this article. All authors provided feedback and changes to the manuscript. G.W., J.M.D., and Z.B. brought together the text and finalized the manuscript.

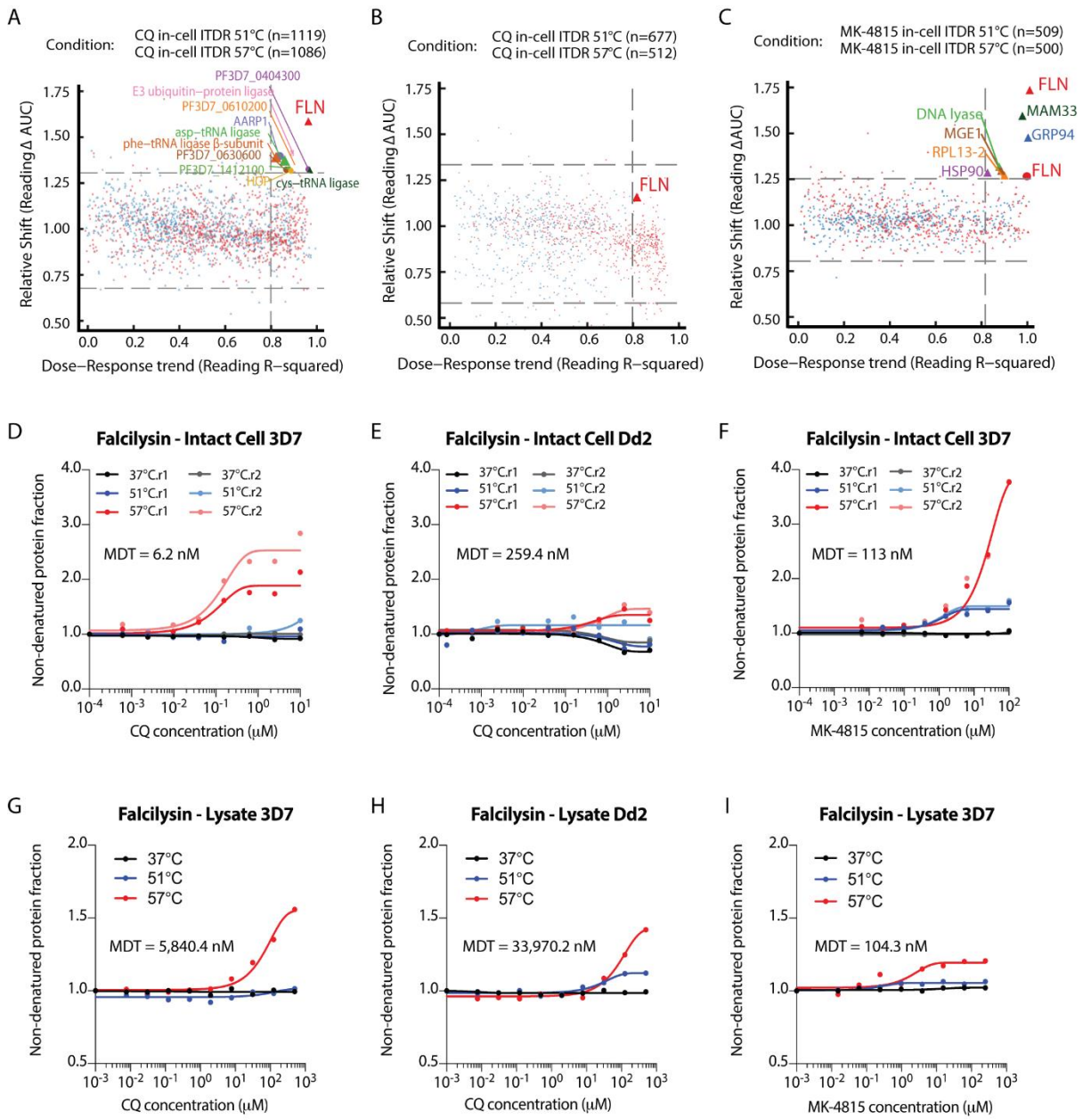

Figure 1. Protein with stability shifts for CQ and MK in 3D7 and Dd2 intact-cell experiments. **(A-C)** Whole proteome analysis in intact-cell ITDR experiments under 0-10 μM of CQ in 3D7 (CQS strain, A), Dd2 (CQR strain, B) or 0-100 μM MK (CQS, C) treatment with thermal challenges at 51°C (circles) or 57°C (triangles). Distribution of protein stabilization is plotted as a function of R^2 value (goodness of curve fit) against ΔAUC (area under the curve of heat-challenged sample normalized against non-denaturing 37°C control) for all proteins detected in the assay. Three times of median absolute deviation (MAD) of ΔAUC in each dataset (MAD × 3) and $R^2 = 0.8$ cutoffs are indicated on the graph. Proteins with significant thermal stabilization are labeled. Thermal stabilization parameters of each protein are described in Table S1. **(D-F)** Thermal stabilization

profile of FLN identified in (A-C). Minimal dose threshold (MDT) stated are from ITDR 57°C, where FLN exhibited the strongest thermal stabilization. Stabilization under thermal challenges [51°C (blue) or 57°C (red)] is plotted relative to no-drug control with non-denaturing control (37°C) plotted in black. Data are from 2 independent experiments **(G-I)** Thermal stabilization profile of FLN in drug- and heat-treated lysate samples. Minimal dose threshold (MDT) stated are from ITDR 57°C, where FLN exhibited the strongest thermal stabilization. Stabilization under thermal challenges [51°C (blue) or 57°C (red)] is plotted relative to no-drug control with non-denaturing control (37°C) plotted in black. Data are from single experiment.

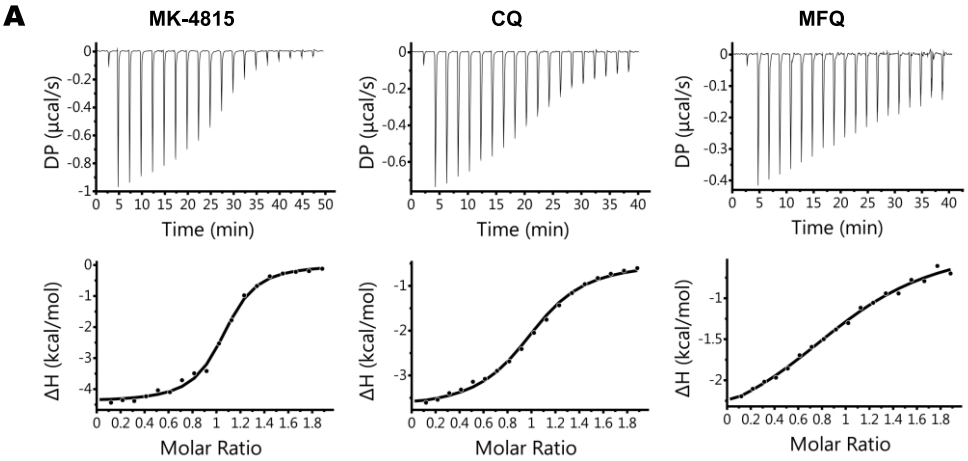

	MK-4815	CQ	MFQ
Number of sites	1.03 ± 0.012	1.0	1.06 ± 0.007
K_d (μM)	1.79 ± 0.30	116 ± 18	26.7 ± 8.60
ΔH (kcal.mol^{-1})	-4.43 ± 0.01	-2.37 ± 0.251	-2.42 ± 0.314
ΔG (kcal.mol^{-1})	-7.85	-5.37	- 6.24
-TΔS (kcal.mol^{-1})	-3.42	-3.0	- 3.82

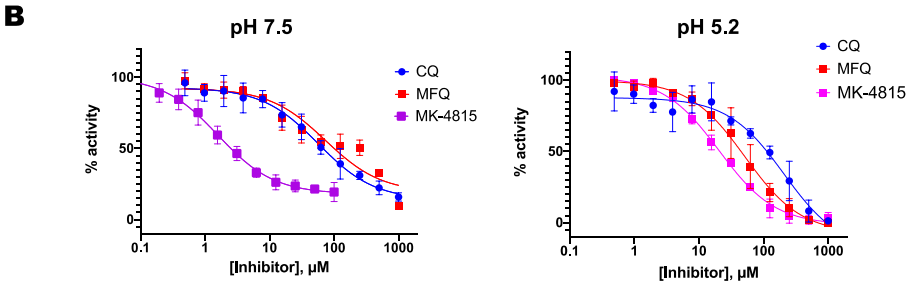

	pH 7.5			pH 5.2		
	CQ	**MFQ**	**MK-4815**	**CQ**	**MFQ**	**MK-4815**
Bottom	13.86	19.05	17.98	-19.37	-7.518	-1.580
Top	92.72	92.30	100.4	87.76	99.83	102.7
IC_{50} (μM)	56.94	73.36	1.596	206.7	51.70	20.51
$logIC_{50}$	1.755	1.865	0.2030	2.315	1.713	1.312
R^2	0.9578	0.8994	0.9712	0.9313	0.9678	0.9916

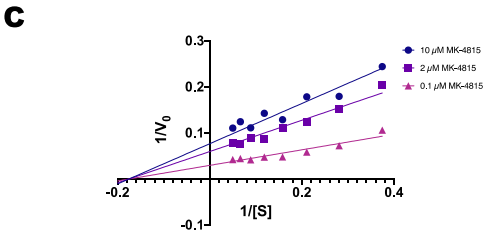

	10 μM MK-4815	2 μM MK-4815	0.1 μM MK-4815
Y intercept ($1/V_{max}$)	0.085	0.052	0.035
X intercept ($-1/K_m$)	-0.18	-0.18	-0.18
Slope (K_m/V_{max})	0.39	0.36	0.09

Figure 2. FLN enzymatic inhibition by CQ, MK-4815, and MFQ. (A) FLN binding thermodynamics to MK-4815, CQ and MFQ measured by isothermal titration calorimetry. The top panels show heat differences upon injection of ligand and lower panels show integrated heats of injection and the best fits (solid line) to a single site binding model. The fitted K_d and thermodynamic values are shown in the Table. **(B)** FLN protease activity inhibition by MK-4815 (purple squares), CQ (blue points) and MFQ (red squares) at pH=7.5 and pH=5.2. Protease activities were measured

in triplicates and normalized for each inhibitor molecule. **(C)** Double reciprocal (Lineweaver-Burk) plot of FLN enzymatic activity in presence of 0.1 µM (pink triangles), 2 µM (purple squares) and 10 µM (blue points) of MK-4815.

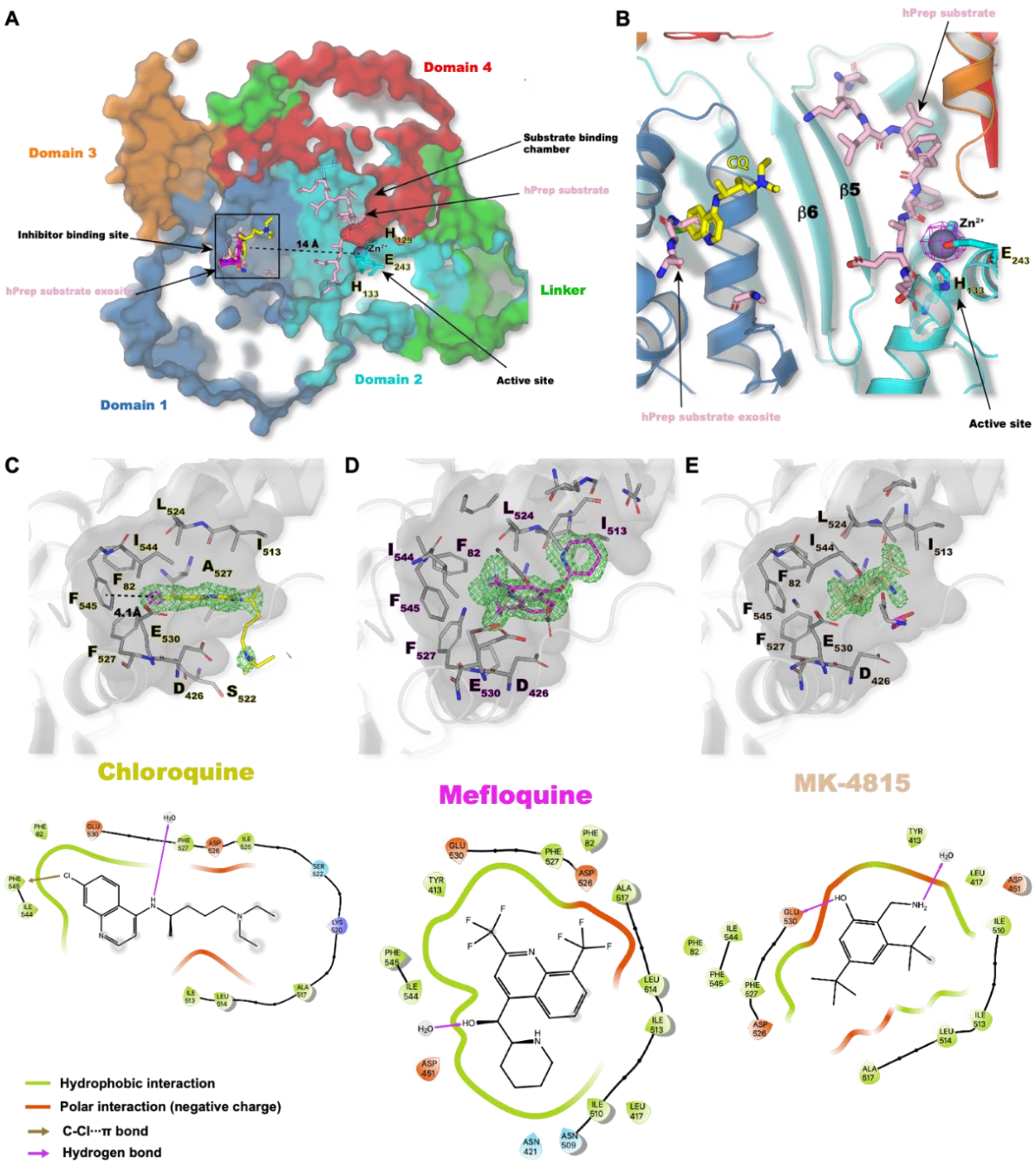

Figure 3. Crystal structures of FLN bound to inhibitors. (**A**) Sliced view of the inner FLN cavity in complex with CQ (yellow sticks). The molecular surface of FLN is shown, colored according to domain 1, residues 1-337, blue, domain 2, residues 338-587, cyan, domain 3, residues 658-990, orange, domain 4, residues 991-1193, red. Linker domain (residues 588-657) connecting domains 2 and 3, is colored in green. Active site residues H_{129}, H_{133} and E_{243} of domain 2 are shown as sticks and colored in cyan. The catalytic zinc ion is shown as a grey sphere. The inhibitors binding pocket

(boxed) is situated at a distance of 14 Å from the catalytic zinc. A model of the complex with the peptide substrate (pink sticks) was obtained by superimposing the hPrep structure (PDB 4NGE) onto the FLN structure. Of note, the inhibitors binding site overlaps with part of the hPrep binding (named hPrep substrate exosite, with sticks colored in purple). (**B**) Close-up view of the FLN inner substrate binding chamber. FLN is shown as ribbons. An anomalous map collected at the zinc absorption edge contoured at 5σ is shown as a purple mesh. The modeled substrate (pink sticks) inferred from superimposition with hPrep, forms an antiparallel β-sheet with strand β5 of FLN. Crystal structures of inhibitors (shown as sticks) bound to FLN (grey molecular surface): CQ (**C,** colored yellow), MFQ (**D,** magenta) and MK-4815 (**E**). Binding pocket residues are shown as sticks and colored in grey. For each bound compound, an Fo-Fc omit map contoured at a level of 3σ is shown as a green mesh. To confirm the position of the Cl atom of CQ, the Fo-Fc omit map for CQ contoured at 5σ is also shown colored in purple. The distance between the Chloride moiety of CQ and the center of the F545 ring is displayed. 2D interactions diagram for each inhibitor are shown below (Schrödinger Maestro Suite).

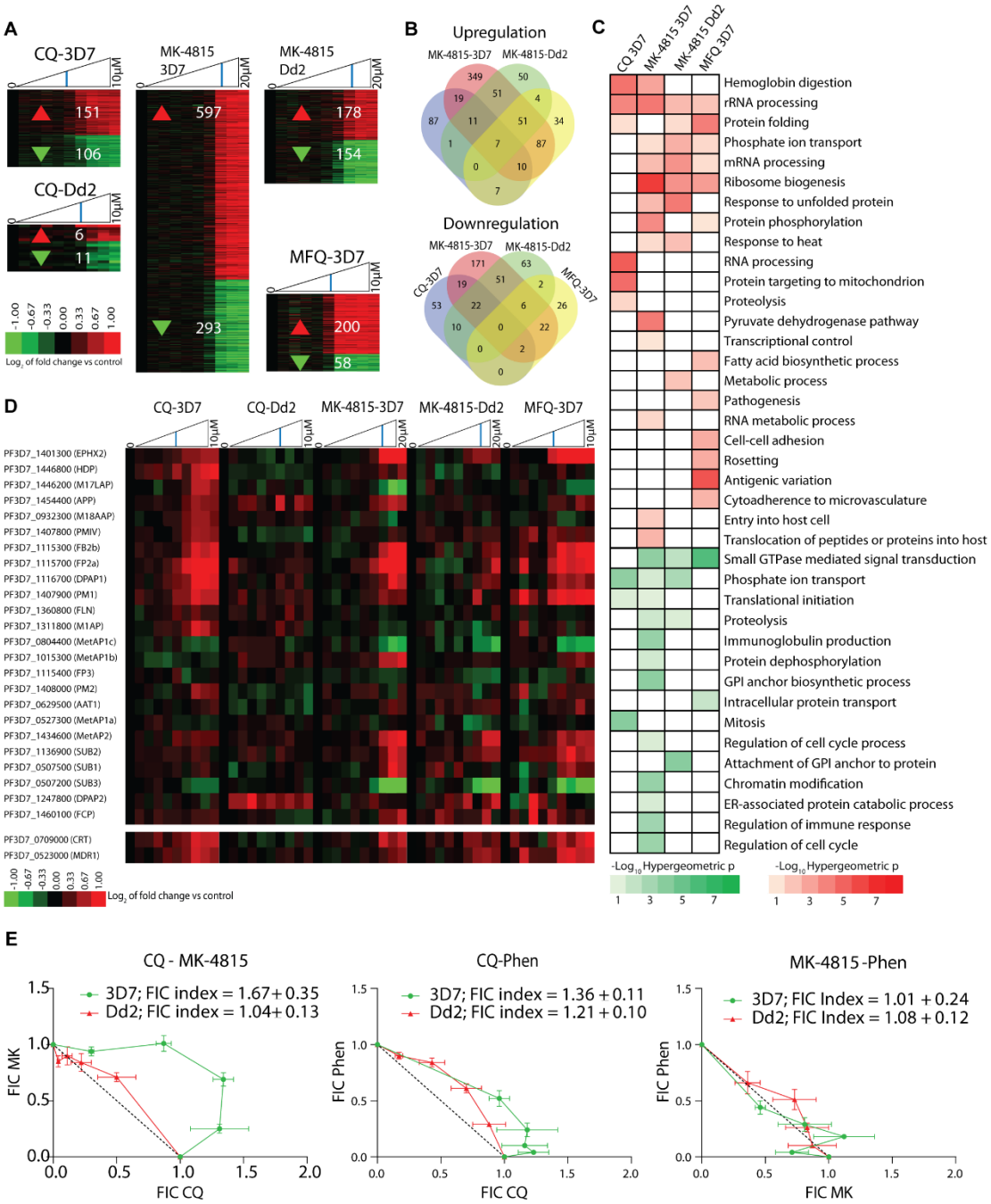

Figure 4. **Characterization of antimalarials MOA with DRTP and isobologram analysis. (A)** Heatmaps of gene that were up- (red) or down- (green) regulated in a dose dependent manner upon treatment with stated compounds for 6 hours. Numbers in red or green represent numbers of genes that were up- or downregulated, respectively. Blue lines on the triangle scale represents the 6 hours drug assay IC_{50}s of the compound. **(B)** Venn diagram of genes similarly up- (top) or down- (bottom)

regulated between antimalarials. **(C)** Significantly over-represented pathways (-log hypergeometric $p > 1.3$) based on genes affected in (A). Overrepresentation of up- and down-regulated pathways are shown in red and green, respectively. Functional gene/pathway annotations listed are based on Gene Ontology Biological Processes (GO-BP) database, with the exception of hemoglobin digestion (Malaria Parasite Metabolic Pathways database). Full list of enriched pathways is available as **Supplementary Data 3**. **(D)** Overview of transcriptional changes in hemoglobin digestion genes and resistance-related genes upon antimalarial treatment. **(E)** Isobologram analysis for the combinations of CQ, MK, and PHEN in 3D7 and Dd2 strains. Isoboles representing FIC index of each drug in combination are plotted across a range of drug pair concentrations. Reference isobole indicating additivity is presented as a black dashed line. FIC indexes stated and error bars representing the standard deviation of the FICs are from 3 biological replicates.

Materials and Methods

Parasite culture

P. falciparum 3D7 and Dd2 cultures were maintained in Malaria Culture Media (MCM) containing RPMI-1640 medium (Gibco) supplemented with 0.25% Albumax II (Gibco), 0.1 mM hypoxanthine (Sigma), 0.2% sodium bicarbonate (Sigma), and 10 mg/L gentamycin. Human blood group O were used for parasite culture and cultures were maintained at 37°C with 5% CO_2, 3% O_2, and 92% N_2. Culture media were replenished daily with freshly packed RBC added to the culture when necessary.

Sample preparation for ITDR MS-CETSA and LC/MS analysis

Samples for intact-cell and lysate ITDR MS-CETSA and LC/MS analysis were prepared as described in Dziekan *et al* [32,33]. For both intact-cell and lysate MS-CETSA, synchronized mid-trophozoite stage (28±4 HPI) culture at 10% parasitaemia and 2% hematocrit was used. In case of intact-cell MS-CETSA, 1 mL of packed blood was loaded on MACS CS column (Milteny Biotech), washed, and eluted. Enriched infected RBC (iRBC)(>80% parasitaemia) were then incubated for 1 hour in MCM at 37°C with agitation for recovery and equilibration. The iRBC were then divided into 10 aliquots (75-90 million cells in 6 mL MCM for each aliquot) and treated with 4-fold dilution series of CQ (Sigma, 10 µM top concentration), MK (100 µM top concentration), or an equivalent volume of their respective solvent at 0.1% concentration, and incubated for 1 hour at 37°C with agitation. Cells were pelleted by centrifugation (2,500 rpm, 5 minutes), washed with PBS, resuspended in 150 µL PBS per aliquot and transferred in 50 µL aliquots to three 96-well plates, each representing different heat challenge temperature (37°C, 51°C, or 58°C). Samples were subjected to thermal challenge for 3 minutes, followed by 3 minutes cooling at 4°C. After heat treatment, 50 µL of lysis buffer (50 mM HEPES pH 7.5, 5 mM beta-glycerophosphate, 0.1 mM Na_3VO_4, 10 mM $MgCl_2$, 2 mM TCEP, and cocktail EDTA-free protease inhibitors (Sigma)) were added to each well. Samples were then subjected to 3 times of freeze/thaw cycle, followed by mechanical shearing and centrifugation (20,000g, 20 minutes, 4°C) to isolate the soluble protein fraction. Protein quantification was then performed with bicinchonidic assay (BCA) protein assay kit (Pierce). In case of lysate MS-CETSA, the parasite culture was pelleted and incubated with 10x volume of 0.1% saponin in PBS (pH 7.2) for 5 minutes. Following centrifugation (2,500g, 5 minutes) the supernatant containing RBC cytosol was removed, whilst intact parasite pellet was washed 3 times with 50 mL of ice-cold PBS. Parasite was then resuspended in 1 mL of lysis buffer and

subjected to 3 times of freeze/thaw cycle, followed by mechanical shearing. Parasite lysate was then centrifuged (20,000g, 20 min, 4°C) and supernatant containing soluble parasite proteins was isolated. Protein concentration was quantified with BCA protein assay kit. Ten aliquots of 20 µg of proteins were added to 4-fold dilution series of CQ (top concentration 500 µM), MK (top concentration 1 mM), or MFQ (Sigma, top concentration 1 mM), incubated at room temperature for 3 minutes, and heated at 37°C, 51°C, or 57°C for 3 minutes followed by 3 minutes cooling at 4°C. The post heating lysates were centrifuged at 20,000g for 20 minutes at 4°C and the supernatant was transferred to a fresh Eppendorf tube for further processing.

Peptide preparation and labeling

Following quantification of lysate and intact-cell samples, the volume equivalent to 20 µg total protein in post heating treatment was aliquoted and incubated with denaturation and reduction buffer containing 100 mM triethylammonium bicarbonate (TEAB, pH 8.5), 20 mM tris(2-carboxyethyl)phosphine) (TCEP, pH 7.0), and 1% (w/v) Rapigest (Waters) at 55°C for 20 minutes, followed by alkylation with 55 mM chloroacetamide (CAA) at room temperature for 30 minutes. Samples were then sequentially digested with Lys-C (0.23 AU LysC/µg of protein, Wako) for 3 hours, followed by trypsin (0.05 µg trypsin/µg of protein) for 18 hours at 37°C. Enzyme activation and Rapigest degradation was performed by incubation with 1% trifluoroacetic acid (TFA, Sigma) for 45 minutes at 37°C and the sample supernatant containing peptides was collected by centrifugation at 20,000g for 10 minutes. The samples were then dried in a centrifugal vacuum evaporator and resolubilized with 200 mM TEAB to 1 µg/µl concentration. Peptides were labeled with TMT10plex Isobaric Label Reagent Set (Thermo Fisher Scientific) according to manufacturer's protocol. Briefly, 4 µg of the digested protein was labeled for at least 1 hour at a condition of pH>6 and then quenched with 1 M Tris (pH 7.4). The labeled samples were subsequently pooled and desalted using a Oasis HLB column (Waters), followed by vacuum drying. Samples were resuspended in 5% (v/v) acetonitrile, 5% (v/v) ammonia and separated using high pH reverse phase Zorbax 300 extend C-18 4.6 mm x 250 mm (Agilent) column and liquid chromatography AKTA Micro system (GE Healthcare) was used for offline sample pre-fractionation into 96 fractions. The fractions were concatenated into 20 fractions and dried with a centrifugal vacuum concentrator.

LC/MS analysis

The dried peptide sample fractions were resuspended in 1% acetonitrile, 0.5% (v/v) acetic acid, and 0.06% TFA in water prior to analysis on LC/MS. Online chromatography was performed using the reverse phase liquid chromatography Dionex 3000 UHPLC system coupled to a Q Exactive HF mass spectrometer (Thermo Fisher Scientific). Each fraction was separated on a 50 cm x 75 µm Easy-Spray analytical column (Thermo Fisher Scientific) in 70 minutes gradient of programmed mixture of mobile phase A (0.1% formic acid) and mobile phase B (99.9% acetonitrile, 0.1% formic acid) to the following gradient ober time: 1-55 min (2-25%), 55-57 min (25-50%), 57-58 min (50-85%), 58-63 min (85%), 63-70 min (2%). MS data were acquired using data-dependent acquisition (DDA) with full scan MS spectra acquired in the range of 350-1550 m/z at a resolution of 70,000 and AGC target of 3e6; Top12 MS^2 35,000 and AGC target of 1e5, and 1e5 isolation window at 1.2 m/z.

Protein identification and quantification

Proteome Discoverer 2.1 software (Thermo Fisher Scientific) was used to perform protein identification and quantification based in the Xcalibur raw files. Raw spectra was submitted for database searching with Sequest HT (Thermo Scientific) search engine using combined Sanger Institute *P. falciparum* 3D7 or Dd2 Coding Sequences database and Uniprot database for human proteins. MS precursor mass tolerance was set at 30 ppm, fragment mass tolerance set at 0.06 Da and maximum missed cleavage sites of 3. Dynamic modifications include oxidation (M), deamidated (NQ), acetylation (N-terminal protein) while static modification includes carbamidomethyl (C). Forward/decoy searches were used for false discovery rate (FDR) estimation. Peptide and peptide spectrum matches (PSMs) with high=FDR 1% and medium=FDR 5% levels were accepted.

Quantitative MS data analysis and MS-CETSA data processing

For downstream analysis, only unique peptides were used for quantification of associated protein abundance and only proteins quantified by at least 3 PSMs were used. Relative abundances of proteins under different compound concentrations were normalized against untreated control and fed into "mineCETSA" R package (available at https://github.com/nkdailingyun/mineCETSA) for data extraction, clean-up, normalization, curve fitting, hit selection, and plotting. The ITDR hit selection considers the global responses from the measured protein population and applies two thresholds: a Median Absolute Deviation scheme where the threshold was set at median $\pm$ 3*MAD

and the R^2 value of curve fitting (indicating goodness of fit) for the selection of the most prominent hits.

Western blotting

Western blots were performed with post-heating lysates generated from the corresponding intact-cell ITDR experiments. 10 µg of protein lysates for each treatment condition was fractionated in 4-15% Mini-Protean TGX protein gels (Bio-Rad) and transferred to PVDF membrane at 40 V overnight. Antibody against FLN (rabbit primary antibody) diluted at 1:5000 in 5% nonfat milk in TBS-Tween (TBST) was used as the primary antibody, and the HRP-conjugated anti-rabbit antibody (Biolegend) diluted at 1:1000 in 5% nonfat milk in TBST was used as the secondary antibody. Blot was developed with Clarity Western ECL system (Bio-Rad), and the image was generated and analyzed using LAS-3000 imager (Fujifilm)

Protein expression and purification

Falcilysin gene (UniProtKB - Q76NL8, gene ID: 814283) coding for residues 59-1193 was synthesized and cloned into pNIC28-Bsa4 downstream a 6xHis tag and TEV cleavage site (pNIC-FLN59-1193). BL21 (DE3) Rosetta T1R cells were transformed with pNIC-FLN59-1193 and grown at 37˚C until OD600 reached 0.6. Protein expression was induced by addition of 0.5 mM IPTG for 16 hours at 16˚C. The bacteria were harvested by centrifugation and cells were resuspended in 100 mM Na HEPES, 500 mM NaCl, 10 mM Imidazole, 10% (v/v) glycerol, 0.5 mM TCEP, pH 7.5, and lysed mechanically (LM20 microfluidizer). Lysate was cleared by centrifugation at 50,000 g for 1 h. Protein was purified by affinity chromatography using Ni-NTA beds (GE Healthcare) and eluted in 20 mM Na HEPES, 500 mM NaCl, 500 mM Imidazole, 10 % (v/v) glycerol, 0.5 mM TCEP, pH 7.5 before size exclusion chromatography using Hiload 16/600 Superdex 200 pg column (GE healthcare) equilibrated in 20 mM NA HEPES, 300 mM NaCl, 10% (v/v) glycerol, 0.5 mM TCEP, pH 7.5. Protein purity was checked by SDS-PAGE, before protein was concentrated to 22 mg.ml-1, flash frozen and stored at -80˚C until use.

Crystallization, Data Collection and Processing

Crystallization conditions for falcilysin were screened with a protein concentration of 22 $mg.ml^{-1}$ using commercial kits (JCSG-plusTM & Morpheus from Molecular Dimensions; Index & PEG/Ion ScreenTM from Hampton Research) using a mosquito crystallization robot (TTP

Labtech). Crystals were obtained after a few days. To obtain the structures of protein-inhibitor complexes, native FLN crystals were soaked with inhibitors at 10 mM concentration for approximately 1.5 h before being flash-frozen in liquid nitrogen. Detailed buffer composition for each structure are presented in **Table S2**. X-ray diffraction intensities were collected at the PXIII beamline (Swiss Light Source, Villigen), integrated and scaled using XDS [68]. Structures were solved with molecular replacement as implemented in the program Phaser [69] using the *P. falciparum* falcilysin ligand-free structure (Goldberg et al, unpublished, PDB access code: 3S5M) as a search probe. Refinement was done using the Phenix package (Adams) and interspersed with manual model correction using Coot [70]. Data collection and refinement statistics are shown in **Table S2**. Structure similarity search was performed using ssm from EBI, (https://www.ebi.ac.uk/msd-srv/ssm/cgi-bin/ssmserver) [71] and returned eight similar structures (r.m.s.d. of 1.78-2.17) all belonging to the M16C metalloprotease family. The volume of the catalytic cavity in the FLN protein was calculated using the 3V webserver [72]. MAD scan was performed to confirm the presence of Zinc in FLN crystal (**Fig. S11**). A dataset was collected at 1.278 Å near Zinc K edge and processed to confirm the presence of Zinc unambiguously (**Table S3**).

Isothermal titration microcalorimetry measurements

Isothermal titration calorimetry data were collected using MICROCAL PEAQ-ITC (Malvern) at 25 °C with 19 injections and 500 rpm stirring speed in buffer 20 mM Na-HEPES pH 7.5, 300 mM NaCl, 10% (*v/v*) glycerol, 0.5 mM TCEP, 1% DMSO. K_d of MK-4815 (1.79 µM) was determined by titrating 200 µL of 100 µM FLN protein with 36.4 µL of 1 mM MK-4815 (**Fig. 2A**). Determination of K_d of CQ to FLN via direct ITC was impossible due to its low binding affinity and limited sensitivity of ITC equipment. Instead, K_d of CQ was estimated by displacement titration [73], titrating 200 µL mixture of 100 µM FLN protein and 200 µM CQ with 36.4 µL of 1 mM MK-4815, which yielded an apparent K_d of 5.5 µM (Fig. 2B). The increase of apparent K_d for MK-4815 from 1.79 µM to 5.5µM was caused by competition of CQ for the same binding site, from which a K_d of 116 µM for CQ was estimated using competitive mode in Marven analysis software. Binding of MK-4815 to FLN was largely inhibited when 200 µL mixture of 100 µM FLN protein and 2 mM CQ was titrated with 36.4 µL of 1 mM MK-4815 (**Fig. S7**).

Enzymatic assay

To determine IC_{50} values of the three inhibitors, FLN activity was monitored using substrate fluorescence quenching at pH 7.5 and pH 5.2 representing values encountered in the

apicoplast/mitochondrion and DV respectively. The FLN protein at a concentration of 20 nM was incubated with 20 µM of substrate peptide [40] (YNHHS↓FFMEE where the arrow indicates the scissile peptide bond) in presence of various concentrations of inhibitors (ranging from 1mM to 0.48 µM for CQ and MFQ and from 100 µM to 0.048 µM for MK-4815). Measurements for each concentration were performed as triplicate. A TECAN 10M plate reader, operated at 336 nm and 495 nm wavelengths for excitation and emission respectively was used to follow FLN protease activity. The reaction was started with automated addition of the enzyme into a mixture of substrate and inhibitor, followed for a total duration of 1 min. The initial velocity was determined automatically using Magellan® software provided by the manufacturer. The V_{max} values obtained were plotted against the log of the inhibitor concentration in GraphPad Prism to obtain the IC_{50} values.

To assess the MOA of MK-4815 and CQ, Michaelis-Menten steady state kinetics parameters were measured in the presence of various inhibitor concentrations. A serial dilution of substrate starting from a maximum value of 20 µM of substrate was incubated with three concentrations of inhibitor ranging from approximately 0.1 to 10 times (2.5 times for CQ due to its lower affinity) of their respective K_d values (0.1 µM, 2 µM and 10 µM of MK-4815 and 1 µM, 50 µM and 250 µM of CQ). The reaction was started with automated addition of the enzyme into a mixture comprising the substrate and inhibitor and followed for 1 min. The initial velocity was determined automatically using Magellan® software. The values of reciprocal velocity were plotted as a function of reciprocal concentration in a Lineweaver-Burk graph.

In vitro **drug sensitivity assay and isobologram analysis**

For isobologram analysis (Fig. **4E**), drug assays were performed in 100 µL volume with mid-ring stage (12±4 HPI) of 3D7 and Dd2 strains at 0.5-1% parasitaemia and 2% hematocrit in a 96-well format. For *in vitro* drug sensitivity assay (**Fig. S10**), trophozoite stage (24±4 HPI) of 3D7 and Dd2 strains were used. The top concentration of compounds used in was 3,200 nM CQ, 16,000 nM MK, 1,000 nM MFQ, and 100 µM o-phenanthroline followed by 2-fold serial dilution and a drug-free control. For isobologram analysis, IC_{50} measurements were conducted for each drug alone and for combinations at fixed volumetric ratio (i.e., Drug A:Drug B ratio – 5:0, 4:1, 3:2, 2:3, 1:4, 0:5). For wash-off assays, parasites were incubated with the compounds for 6 hours, followed by 2x washes with MCM to remove the compounds completely from the MCM, followed by 42 hours incubation (total 48 hours incubation). Following 48 hours incubation, supernatant was removed and iRBCs were stained with 50 µL of 8 µM Hoechst 33342 in PBS (pH 7.2) for 15 minutes at 37°C, followed

by addition of 200 µL of PBS. Results readout was conducted with the LSR Fortessa X-20 Flow Cytometer (BD Biosciences) equipped with HTS sampler using UV laser (355 nm). Raw FCS data was gated and analyzed with FACS DIVA software. Linear regression analysis of dose-response curves and IC_{50} determination was subsequently done using GraphPad Prism 8 (Graphpad Software). Isobologram analysis was conducted according to Loewe additivity model, where the sum of fractional inhibitory concentrations (ΣFIC_{50}) for the two compounds in a combination is a measure of additivity, synergism, or antagonism. The combination with $\Sigma FIC_{50}>1$ are considered antagonistic, <1 synergistic, and equal to 1 is additive [74].

Drug treatment and RNA extraction for DRTP

For DRTP experiment, sorbitol-synchronized mid-trophozoite stage (28±4 HPI) of 3D7 and Dd2 culture were used. Parasite culture was divided into 10 well in two 6-well plates with each well containing 6 mL of culture at 3% parasitaemia and 2% hematocrit and treated with 4-fold dilution series of CQ (10 µM top concentration), MK (20 µM top concentration), MFQ (10 µM top concentration) and an equivalent volume of DMSO at 0.1% concentration and incubated for 6 hours at 37°C with 5% CO_2, 3% O_2, and 92% N_2. Following incubation, the samples were harvested and centrifuged at 2,500 rpm for 5 minutes. After removal of supernatant, 1 mL of Trizol reagent (Invitrogen) was added to the iRBC pellet, followed by vigorous shaking and incubation at 37°C for 10 minutes. Following lysis, 200 µL of chloroform was added and the mixture was incubated in ice for 5 minutes with periodical shaking. Samples were then centrifuged at 12,000g for 15 minutes at room temperature to separate the organic and aqueous phases. Five hundred µl of the aqueous phase was collected and RNA was purified by using the Direct-zol-96 RNA kits (Zymo Research) as per manufacturer's protocol.

cDNA synthesis, SMART amplification, and microarray analysis

cDNA synthesis, Switching Mechanism at 5` End of RNA Template (SMART) amplification of double stranded cDNA, and microarray hybridization was performed as previously described by Bozdech *et al.* [75]. Briefly, 500 ng of total RNA was used as the input for reverse transcription using SuperScript II (Invtirogen). The cDNA product was then amplified using SMART-PCR containing aminoallyl-dUTP and dNTPs. Four µg of SMART-amplified samples were then labelled with Cy5. On the other hand, reference cDNA generated from pooling together RNA from all IDC stages of 3D7 was labelled with Cy3. Equal amounts of Cy3- and Cy5-labelled products were then hybridized

onto a microarray chip containing 10,265 probes covering ~5000 genes in the *P. falciparum* genome. Fluorescence intensity from labelled samples were scanned with Tecan Powerscanner open-format microarray scanner. Background subtraction, normalization, and filtering of raw signal intensities for each array were done using the R package 'limma' [76].

DRTP data analysis, functional pathway enrichment, and semantic proximity analysis

Selection of dose-dependent up- or downregulation was performed with the 'mineCETSA' package with modifications. Gene expression $\log_2$ ratios of treated samples were first normalized and converted into fold change of gene expression against untreated samples for each drug. The fold-change expression data were then fed into 'mineCETSA' package for data normalization and fitting. Following curve fitting, dose-dependent up- and down-regulation were then selected using the following criteria: 1) at least 30% fold change increase compared to untreated control in the top 3 highest concentration, 2) goodness of sigmoidal curve fitting (R^2) value greater than 0.8 in 2 biological replicates, and 3) unidirectionality of each gene response in 2 biological replicates. Genes showing dose-dependent expression changes were then subjected to functional pathway enrichment analysis to calculate functionally enriched pathways in a given dataset using the functional gene annotation from Gene Ontology (GO) and Malaria Parasite Metabolic Pathway (MPMP) databases as described previously [77]. Over-representation of pathways as compared to their respective frequency in the genome was calculated based on hypergeometric test ($p<0.05$).

References

1 World Health Organization. World Malaria Report 2019. (Geneva, Switzerland, 2019).

2 Ashley, E. A. *et al.* Spread of artemisinin resistance in Plasmodium falciparum malaria. *N. Engl. J. Med.* **371**, 411-423, doi:10.1056/NEJMoa1314981 (2014).

3 Dondorp, A. M. *et al.* Artemisinin resistance in Plasmodium falciparum malaria. *N. Engl. J. Med.* **361**, 455-467, doi:10.1056/NEJMoa0808859 (2009).

4 van der Pluijm, R. W. *et al.* Determinants of dihydroartemisinin-piperaquine treatment failure in Plasmodium falciparum malaria in Cambodia, Thailand, and Vietnam: a prospective clinical, pharmacological, and genetic study. *Lancet Infect Dis* **19**, 952-961, doi:10.1016/s1473-3099(19)30391-3 (2019).

5 Phyo, A. P. *et al.* Declining Efficacy of Artemisinin Combination Therapy Against P. Falciparum Malaria on the Thai-Myanmar Border (2003-2013): The Role of Parasite Genetic Factors. *Clin Infect Dis* **63**, 784-791, doi:10.1093/cid/ciw388 (2016).

6 Guiguemde, W. A. *et al.* Global phenotypic screening for antimalarials. *Chemistry & biology* **19**, 116-129, doi:10.1016/j.chembiol.2012.01.004 (2012).

7 Cowell, A. N. & Winzeler, E. A. Advances in omics-based methods to identify novel targets for malaria and other parasitic protozoan infections. *Genome Med.* **11**, 63, doi:10.1186/s13073-019-0673-3 (2019).
8 Wahlgren, M. & Perlmann, P. *Malaria: molecular and clinical aspects*. (CRC Press, 2003).
9 Krafts, K., Hempelmann, E. & Skórska-Stania, A. From methylene blue to chloroquine: a brief review of the development of an antimalarial therapy. *Parasitology research* **111**, 1-6, doi:10.1007/s00436-012-2886-x (2012).
10 Jensen, M. & Mehlhorn, H. Seventy-five years of Resochin in the fight against malaria. *Parasitology research* **105**, 609-627, doi:10.1007/s00436-009-1524-8 (2009).
11 Krugliak, M., Zhang, J. & Ginsburg, H. Intraerythrocytic Plasmodium falciparum utilizes only a fraction of the amino acids derived from the digestion of host cell cytosol for the biosynthesis of its proteins. *Mol Biochem Parasitol* **119**, 249-256, doi:10.1016/s0166-6851(01)00427-3 (2002).
12 Aft, R. L. & Mueller, G. C. Hemin-mediated oxidative degradation of proteins. *J Biol Chem* **259**, 301-305 (1984).
13 Aft, R. L. & Mueller, G. C. Hemin-mediated DNA strand scission. *J Biol Chem* **258**, 12069-12072 (1983).
14 Chou, A. C. & Fitch, C. D. Mechanism of hemolysis induced by ferriprotoporphyrin IX. *J Clin Invest* **68**, 672-677, doi:10.1172/jci110302 (1981).
15 Klouche, K. *et al.* Mechanism of in vitro heme-induced LDL oxidation: effects of antioxidants. *Eur J Clin Invest* **34**, 619-625, doi:10.1111/j.1365-2362.2004.01395.x (2004).
16 Shinar, E. & Rachmilewitz, E. A. Oxidative denaturation of red blood cells in thalassemia. *Semin Hematol* **27**, 70-82 (1990).
17 Vincent, S. H. Oxidative effects of heme and porphyrins on proteins and lipids. *Semin Hematol* **26**, 105-113 (1989).
18 Pandey, A. V. *et al.* Hemozoin formation in malaria: a two-step process involving histidine-rich proteins and lipids. *Biochem Biophys Res Commun* **308**, 736-743, doi:10.1016/s0006-291x(03)01465-7 (2003).
19 Fitch, C. D., Cai, G. Z., Chen, Y. F. & Shoemaker, J. D. Involvement of lipids in ferriprotoporphyrin IX polymerization in malaria. *Biochim Biophys Acta* **1454**, 31-37, doi:10.1016/s0925-4439(99)00017-4 (1999).
20 Pisciotta, J. M. *et al.* The role of neutral lipid nanospheres in Plasmodium falciparum haem crystallization. *Biochem J* **402**, 197-204, doi:10.1042/bj20060986 (2007).
21 Sullivan, D. J., Jr., Gluzman, I. Y. & Goldberg, D. E. Plasmodium hemozoin formation mediated by histidine-rich proteins. *Science* **271**, 219-222, doi:10.1126/science.271.5246.219 (1996).
22 Chugh, M. *et al.* Protein complex directs hemoglobin-to-hemozoin formation in Plasmodium falciparum. *Proceedings of the National Academy of Sciences* **110**, 5392-5397, doi:10.1073/pnas.1218412110 (2013).
23 Jani, D. *et al.* HDP-a novel heme detoxification protein from the malaria parasite. *PLoS Pathog* **4**, e1000053, doi:10.1371/journal.ppat.1000053 (2008).
24 Nakatani, K., Ishikawa, H., Aono, S. & Mizutani, Y. Heme-binding properties of heme detoxification protein from Plasmodium falciparum. *Biochem Biophys Res Commun* **439**, 477-480, doi:10.1016/j.bbrc.2013.08.100 (2013).
25 Kapishnikov, S. *et al.* Unraveling heme detoxification in the malaria parasite by in situ correlative X-ray fluorescence microscopy and soft X-ray tomography. *Sci Rep* **7**, 7610, doi:10.1038/s41598-017-06650-w (2017).

26 Foley, M. & Tilley, L. Quinoline antimalarials: mechanisms of action and resistance and prospects for new agents. *Pharmacol Ther* **79**, 55-87, doi:10.1016/s0163-7258(98)00012-6 (1998).
27 Weissbuch, I. & Leiserowitz, L. Interplay between malaria, crystalline hemozoin formation, and antimalarial drug action and design. *Chem Rev* **108**, 4899-4914, doi:10.1021/cr078274t (2008).
28 Olafson, K. N., Ketchum, M. A., Rimer, J. D. & Vekilov, P. G. Mechanisms of hematin crystallization and inhibition by the antimalarial drug chloroquine. *Proc Natl Acad Sci U S A* **112**, 4946-4951, doi:10.1073/pnas.1501023112 (2015).
29 Sidhu, A. B., Verdier-Pinard, D. & Fidock, D. A. Chloroquine resistance in Plasmodium falciparum malaria parasites conferred by pfcrt mutations. *Science* **298**, 210-213, doi:10.1126/science.1074045 (2002).
30 Ecker, A., Lehane, A. M., Clain, J. & Fidock, D. A. PfCRT and its role in antimalarial drug resistance. *Trends in parasitology* **28**, 504-514, doi:10.1016/j.pt.2012.08.002 (2012).
31 Powles, M. A. *et al.* MK-4815, a potential new oral agent for treatment of malaria. *Antimicrob Agents Chemother* **56**, 2414-2419, doi:10.1128/aac.05326-11 (2012).
32 Dziekan, J. M. *et al.* Cellular thermal shift assay for the identification of drug-target interactions in the Plasmodium falciparum proteome. *Nat Protoc*, doi:10.1038/s41596-020-0310-z (2020).
33 Dziekan, J. M. *et al.* Identifying purine nucleoside phosphorylase as the target of quinine using cellular thermal shift assay. *Sci. Transl. Med.* **11**, doi:10.1126/scitranslmed.aau3174 (2019).
34 Eggleson, K. K., Duffin, K. L. & Goldberg, D. E. Identification and characterization of falcilysin, a metallopeptidase involved in hemoglobin catabolism within the malaria parasite Plasmodium falciparum. *The Journal of biological chemistry* **274**, 32411-32417, doi:10.1074/jbc.274.45.32411 (1999).
35 Murata, C. E. & Goldberg, D. E. Plasmodium falciparum falcilysin: a metalloprotease with dual specificity. *J. Biol. Chem.* **278**, 38022-38028, doi:10.1074/jbc.M306842200 (2003).
36 Martinez Molina, D. *et al.* Monitoring drug target engagement in cells and tissues using the cellular thermal shift assay. *Science* **341**, 84-87, doi:10.1126/science.1233606 (2013).
37 Wellems, T. E. *et al.* Chloroquine resistance not linked to mdr-like genes in a Plasmodium falciparum cross. *Nature* **345**, 253-255, doi:10.1038/345253a0 (1990).
38 Powles, M. A. *et al.* MK-4815, a potential new oral agent for treatment of malaria. *Antimicrob. Agents Chemother.* **56**, 2414-2419, doi:10.1128/AAC.05326-11 (2012).
39 Dai, L. *et al.* Horizontal Cell Biology: Monitoring Global Changes of Protein Interaction States with the Proteome-Wide Cellular Thermal Shift Assay (CETSA). *Annu. Rev. Biochem.*, doi:10.1146/annurev-biochem-062917-012837 (2019).
40 Murata, C. E. & Goldberg, D. E. Plasmodium falciparum falcilysin: an unprocessed food vacuole enzyme. *Mol Biochem Parasitol* **129**, 123-126, doi:10.1016/s0166-6851(03)00098-7 (2003).
41 Matter, H. *et al.* Evidence for C-Cl/C-Br...pi interactions as an important contribution to protein-ligand binding affinity. *Angewandte Chemie (International ed. in English)* **48**, 2911-2916, doi:10.1002/anie.200806219 (2009).
42 Johnson, K. A. *et al.* The closed structure of presequence protease PreP forms a unique 10,000 Angstroms3 chamber for proteolysis. *The EMBO journal* **25**, 1977-1986, doi:10.1038/sj.emboj.7601080 (2006).

43 Rocamora, F. *et al.* Oxidative stress and protein damage responses mediate artemisinin resistance in malaria parasites. *PLoS Pathog.* **14**, e1006930, doi:10.1371/journal.ppat.1006930 (2018).

44 Reiling, S. J., Krohne, G., Friedrich, O., Geary, T. G. & Rohrbach, P. Chloroquine exposure triggers distinct cellular responses in sensitive versus resistant Plasmodium falciparum parasites. *Sci. Rep.* **8**, 11137, doi:10.1038/s41598-018-29422-6 (2018).

45 Ponpuak, M. *et al.* A role for falcilysin in transit peptide degradation in the Plasmodium falciparum apicoplast. *Mol. Microbiol.* **63**, 314-334, doi:10.1111/j.1365-2958.2006.05443.x (2007).

46 Goldberg, D. E. in *Malaria: Drugs, Disease and Post-genomic Biology* (eds R. W. Compans *et al.*) 275-291 (Springer Berlin Heidelberg, 2005).

47 Geary, T. G., Jensen, J. B. & Ginsburg, H. Uptake of [3H]chloroquine by drug-sensitive and -resistant strains of the human malaria parasite Plasmodium falciparum. *Biochem Pharmacol* **35**, 3805-3812, doi:10.1016/0006-2952(86)90668-4 (1986).

48 Bray, P. G. *et al.* PfCRT and the trans-vacuolar proton electrochemical gradient: regulating the access of chloroquine to ferriprotoporphyrin IX. *Molecular microbiology* **62**, 238-251, doi:10.1111/j.1365-2958.2006.05368.x (2006).

49 Sullivan, D. J., Jr., Gluzman, I. Y., Russell, D. G. & Goldberg, D. E. On the molecular mechanism of chloroquine's antimalarial action. *Proc Natl Acad Sci U S A* **93**, 11865-11870, doi:10.1073/pnas.93.21.11865 (1996).

50 Bray, P. G., Mungthin, M., Ridley, R. G. & Ward, S. A. Access to hematin: the basis of chloroquine resistance. *Molecular pharmacology* **54**, 170-179, doi:10.1124/mol.54.1.170 (1998).

51 Fidock, D. A. *et al.* Mutations in the P. falciparum digestive vacuole transmembrane protein PfCRT and evidence for their role in chloroquine resistance. *Molecular cell* **6**, 861-871, doi:10.1016/s1097-2765(05)00077-8 (2000).

52 Sanchez, C. P. *et al.* Differences in trans-stimulated chloroquine efflux kinetics are linked to PfCRT in Plasmodium falciparum. *Mol. Microbiol.* **64**, 407-420, doi:10.1111/j.1365-2958.2007.05664.x (2007).

53 Sanchez, C. P., Stein, W. & Lanzer, M. Trans stimulation provides evidence for a drug efflux carrier as the mechanism of chloroquine resistance in Plasmodium falciparum. *Biochemistry* **42**, 9383-9394, doi:10.1021/bi034269h (2003).

54 Fitch, C. D. Ferriprotoporphyrin IX, phospholipids, and the antimalarial actions of quinoline drugs. *Life sciences* **74**, 1957-1972, doi:10.1016/j.lfs.2003.10.003 (2004).

55 Saliba, K. J., Folb, P. I. & Smith, P. J. Role for the plasmodium falciparum digestive vacuole in chloroquine resistance. *Biochemical pharmacology* **56**, 313-320, doi:10.1016/s0006-2952(98)00140-3 (1998).

56 Famin, O. & Ginsburg, H. Differential effects of 4-aminoquinoline-containing antimalarial drugs on hemoglobin digestion in Plasmodium falciparum-infected erythrocytes. *Biochem. Pharmacol.* **63**, 393-398 (2002).

57 Zhang, Y. Inhibition of hemoglobin degradation in Plasmodium falciparum by chloroquine and ammonium chloride. *Experimental parasitology* **64**, 322-327, doi:10.1016/0014-4894(87)90042-7 (1987).

58 Fitch, C. D. Involvement of heme in the antimalarial action of chloroquine. *Transactions of the American Clinical and Climatological Association* **109**, 97-105; discussion 105-106 (1998).

59 Zarchin, S., Krugliak, M. & Ginsburg, H. Digestion of the host erythrocyte by malaria parasites is the primary target for quinoline-containing antimalarials. *Biochem. Pharmacol.* **35**, 2435-2442 (1986).
60 Birrell, G. W. *et al.* Multi-omic Characterization of the Mode of Action of a Potent New Antimalarial Compound, JPC-3210, Against Plasmodium falciparum. *Molecular & cellular proteomics : MCP* **19**, 308-325, doi:10.1074/mcp.RA119.001797 (2020).
61 Creek, D. J. *et al.* Metabolomics-Based Screening of the Malaria Box Reveals both Novel and Established Mechanisms of Action. *Antimicrob. Agents Chemother.* **60**, 6650-6663, doi:10.1128/aac.01226-16 (2016).
62 McFadden, G. I. & Yeh, E. The apicoplast: now you see it, now you don't. *International journal for parasitology* **47**, 137-144, doi:10.1016/j.ijpara.2016.08.005 (2017).
63 Martinez Molina, D. & Nordlund, P. The Cellular Thermal Shift Assay: A Novel Biophysical Assay for In Situ Drug Target Engagement and Mechanistic Biomarker Studies. *Annu. Rev. Pharmacol. Toxicol.* **56**, 141-161, doi:10.1146/annurev-pharmtox-010715-103715 (2016).
64 Mateus, A. *et al.* Thermal proteome profiling in bacteria: probing protein state in vivo. *Mol. Syst. Biol.* **14**, e8242, doi:10.15252/msb.20188242 (2018).
65 Herneisen, A. L. *et al.* Identifying the Target of an Antiparasitic Compound in Toxoplasma Using Thermal Proteome Profiling. *ACS Chemical Biology* **15**, 1801-1807, doi:10.1021/acschembio.0c00369 (2020).
66 Favuzza, P. *et al.* Dual Plasmepsin-Targeting Antimalarial Agents Disrupt Multiple Stages of the Malaria Parasite Life Cycle. *Cell host & microbe* **27**, 642-658.e612, doi:10.1016/j.chom.2020.02.005 (2020).
67 Lu, K.-Y. *et al.* Plasmodium chaperonin TRiC/CCT identified as a target of the antihistamine clemastine using parallel chemoproteomic strategy. *Proceedings of the National Academy of Sciences* **117**, 5810-5817, doi:10.1073/pnas.1913525117 (2020).
68 Kabsch, W. XDS. *Acta crystallographica. Section D, Biological crystallography* **66**, 125-132, doi:10.1107/s0907444909047337 (2010).
69 McCoy, A. J. *et al.* Phaser crystallographic software. *Journal of applied crystallography* **40**, 658-674, doi:10.1107/s0021889807021206 (2007).
70 Emsley, P. & Cowtan, K. Coot: model-building tools for molecular graphics. *Acta crystallographica. Section D, Biological crystallography* **60**, 2126-2132, doi:10.1107/s0907444904019158 (2004).
71 Krissinel, E. & Henrick, K. Secondary-structure matching (SSM), a new tool for fast protein structure alignment in three dimensions. *Acta crystallographica. Section D, Biological crystallography* **60**, 2256-2268, doi:10.1107/s0907444904026460 (2004).
72 Voss, N. R. & Gerstein, M. 3V: cavity, channel and cleft volume calculator and extractor. *Nucleic acids research* **38**, W555-562, doi:10.1093/nar/gkq395 (2010).
73 Sigurskjold, B. W. Exact analysis of competition ligand binding by displacement isothermal titration calorimetry. *Analytical biochemistry* **277**, 260-266, doi:10.1006/abio.1999.4402 (2000).
74 Foucquier, J. & Guedj, M. Analysis of drug combinations: current methodological landscape. *Pharmacol Res Perspect* **3**, e00149, doi:10.1002/prp2.149 (2015).
75 Bozdech, Z., Mok, S. & Gupta, A. P. DNA microarray-based genome-wide analyses of Plasmodium parasites. *Methods Mol. Biol.* **923**, 189-211, doi:10.1007/978-1-62703-026-7_13 (2013).
76 Smyth, G. K. Linear models and empirical bayes methods for assessing differential expression in microarray experiments. *Stat Appl Genet Mol Biol* **3**, Article3, doi:10.2202/1544-6115.1027 (2004).

77 Gupta, A. P. *et al.* Histone 4 lysine 8 acetylation regulates proliferation and host-pathogen interaction in Plasmodium falciparum. *Epigenetics & chromatin* **10**, 40, doi:10.1186/s13072-017-0147-z (2017).